Magnetic PDF-analysis: a real-space probe of static and dynamic short-range spin-spin correlations

Henry E. Fischer

Institut Laue-Langevin, Grenoble

101st ILL Scientific Council
9:00 Friday 8 November 2019

mPDF-analysis
Henry E. Fischer
Diffraction basics
PDF-analysis
PDF examples
UO_2
carbon
mPDF-analysis
mPDF examples
$SrGd_2O_4$
Gd_2O_3
$Gd_2Ir_2O_7$
EuPtGe
$TmMgGaO_4$
$SrNd_2O_4$
mPDF fans
Conclusions
Table of Contents

Diffraction Basics

Schematic of a diffraction measurement (mono-λ)

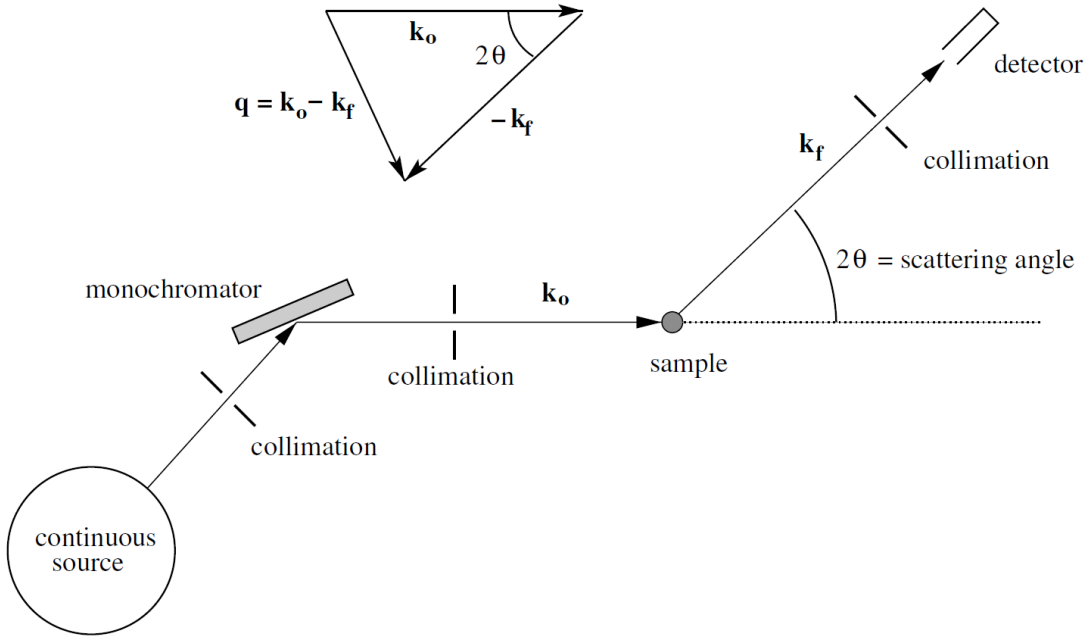

Quanta (*e.g.* x-rays or neutrons) of incident wavevector $\mathbf{k}_o$ and incident energy E_o are scattered by a sample through a scattering angle 2θ thus losing kinetic energy $\hbar\omega = E_o - E_f$ and momentum $\hbar\mathbf{q}$ where $\mathbf{q} = \mathbf{k}_o - \mathbf{k}_f$ is the wavevector transfer or scattering vector.

mPDF-analysis
Henry E. Fischer
Diffraction basics
PDF-analysis
PDF examples
UO_2
carbon
mPDF-analysis
mPDF examples
$SrGd_2O_4$
Gd_2O_3
$Gd_2Ir_2O_7$
EuPtGe
$TmMgGaO_4$
$SrNd_2O_4$
mPDF fans
Conclusions
Table of Contents

Schematic of a diffraction measurement (mono-λ)

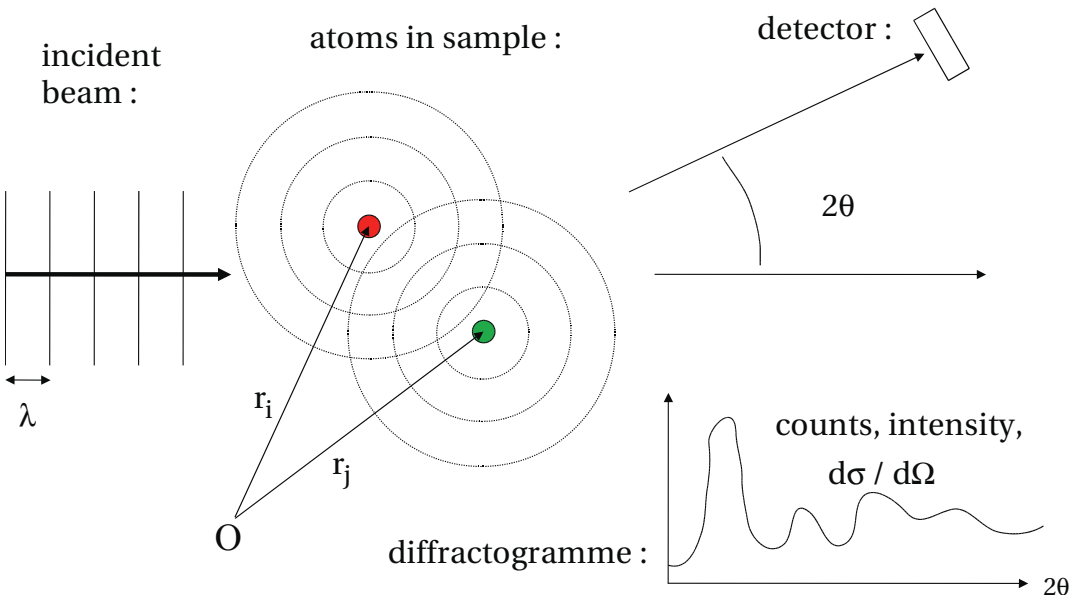

The spherical waves of scattering amplitude from all the atoms in a given quantum's coherence volume ($\phi \sim 100$ Å) interfere with each other at the detector, producing a diffraction pattern as a function of the scattering angle 2θ or the scalar $q = (4\pi/\lambda)\ \sin(\theta)$.

Coherence volume of a neutron wavepacket

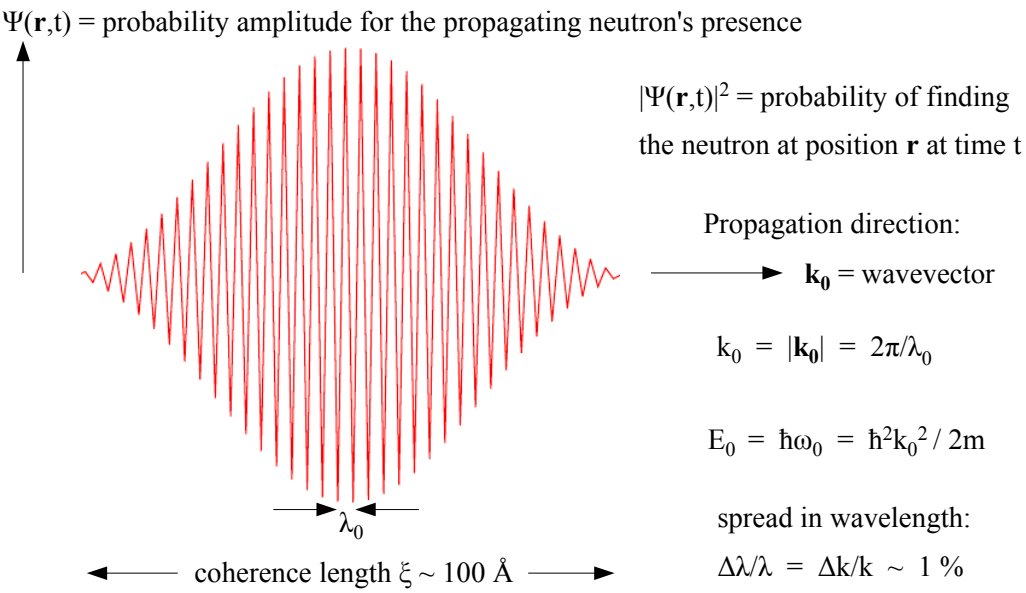

A Gaussian wavepacket of energy $\hbar\omega_0$ is localized in position and wavevector for each dimension as *e.g.* $\Delta x\ \Delta k_x = \hbar/2$ and propagates with group velocity $v_g = \mathrm{d}\omega/\mathrm{d}k$. The diffracting neutron has "seen" only the 100,000 or so atoms that "felt" its wavefunction $\Psi(\mathbf{r}, t)$ within the coherence volume $V_{\mathrm{coh}} \sim \xi^3$ of the diffraction event.

mPDF-analysis
Henry E. Fischer
Diffraction basics
PDF-analysis
PDF examples
UO_2
carbon
mPDF-analysis
mPDF examples
$SrGd_2O_4$
Gd_2O_3
$Gd_2Ir_2O_7$
EuPtGe
$TmMgGaO_4$
$SrNd_2O_4$
mPDF fans
Conclusions
Table of Contents

PDF-analysis

Total scattering, $S(\mathbf{q},\omega)$, and time scales

A diffraction pattern integrates over all sample-neutron E-transfers:

$$\left.\frac{d\sigma}{d\Omega}(\mathbf{q})\right|_{\text{meas}} = \int_{-\infty}^{E_o} d(\hbar\omega)\,\frac{\sigma}{4\pi}\,\frac{k_f}{k_o}\,N\,S(\mathbf{q},\omega)\ ,$$

and therefore represents a quasi-instantaneous "snapshot" of the sample's structure, given the very small coherence time $\tau_{coh} \sim \hbar/(4E_o)$ (from $\Delta t\,\Delta E = \hbar/2$), as ensemble-averaged over coherence volumes.

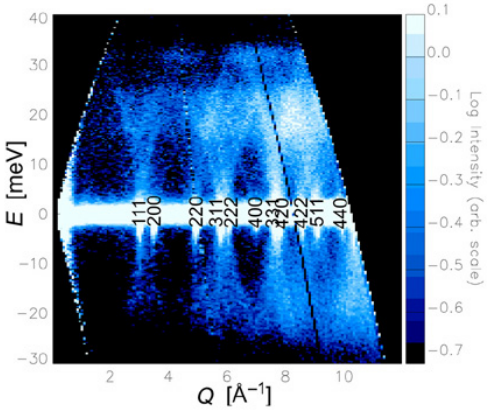

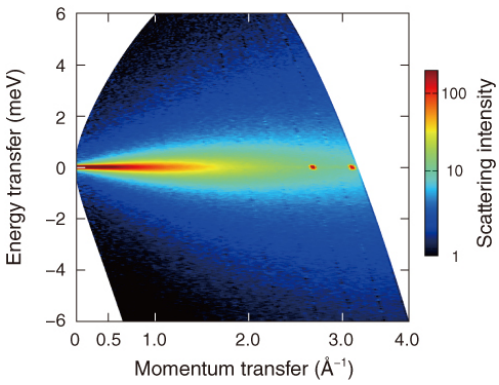

Rietveld refinement of *elastic* Bragg peaks disregards the inelastic scattering containing information about *dynamic* atomic correlations (*e.g.* phonons) and represents the sample's time-averaged structure.

Total scattering, diffuse intensity, and length scales

In addition, the refinement of diffraction intensity only at Bragg-peak positions neglects the inter-peak diffuse intensity, which when elastic represents time-averaged or *static* local atomic correlations.

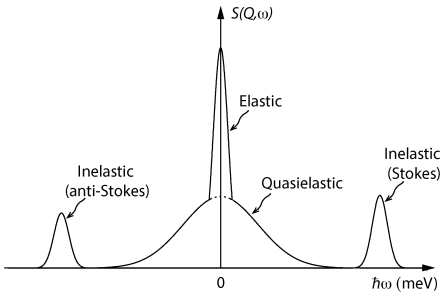

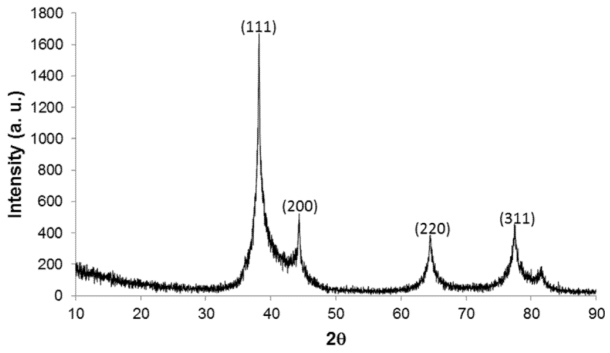

By neglecting the diffuse intensity between (and "under") Bragg peaks, Rietveld refinement additionally performs a spatial average over each neutron coherence volume, resulting in a time+space averaged picture of the sample's structure, which is very useful for crystallography.

By retaining all the original information in the differential cross-section $(d\sigma/d\Omega)(\mathbf{q})$ measured via diffraction, total-scattering represents an ensemble average of quasi-instantaneous snapshots of local structures (*i.e.* within each neutron coherence volume) throughout the sample.

$S(q)$ for a glass or liquid (isotropic, monoatomic)

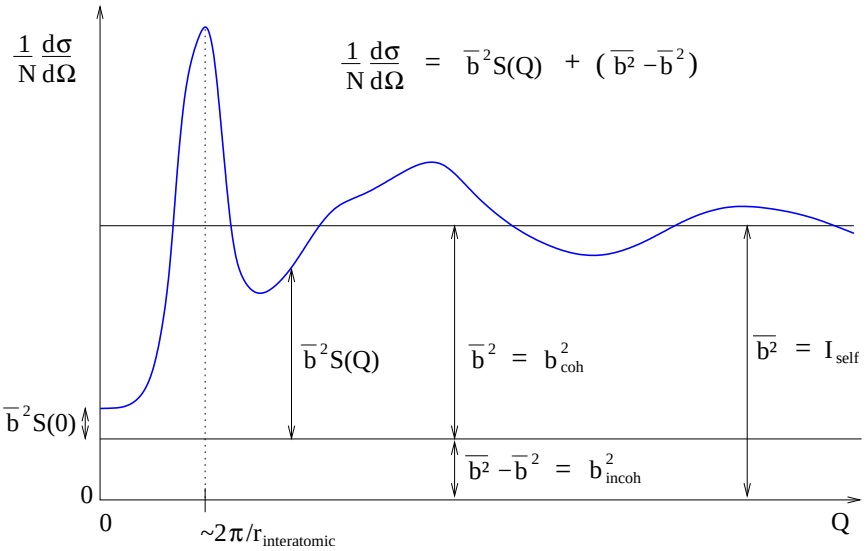

where $\overline{b} = b_{\rm coh}$, and where $(\overline{b^2} - \overline{b}^2) = var(b)$ is simply the variance of scattering lengths throughout the sample. The alternative expression:

$$\frac{1}{N}\left[\frac{d\sigma}{d\Omega}(q)\right] = \overline{b}^2\,[S(q)-1] + \overline{b^2}$$

comprises a "distinct" term (interference between different atoms) and a "self" term (self-interference from individual atoms).

Real-space functions (monoatomic case)

Fourier transform gives the *pair-distribution function* $g(r)$ which is proportional to the probability of finding an atom at a distance r from an average atom taken as the origin:

$$g(r) - 1 = \frac{1}{2\pi^2 r \rho_o}\int_0^\infty q\,[S(q)-1]\sin(qr)\,dq$$

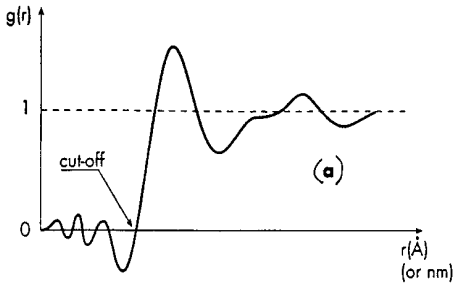

in addition to the density function $D(r)$ (also called $G(r)$) used for "PDF-analysis":

$$\mathrm{PDF}(r) = G(r) = D(r) = 4\pi r\rho_o\,[g(r)-1]$$

$$= \frac{2}{\pi}\int_0^\infty q\,[S(q)-1]\sin(qr)\,dq$$

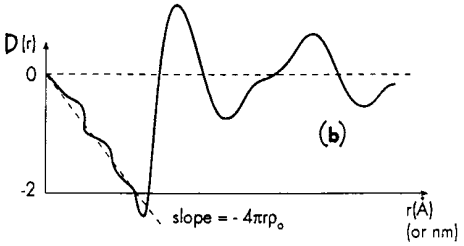

as well as the radial distribution function:

$$\mathrm{RDF}(r) = 4\pi r^2 \rho_o\, g(r)$$

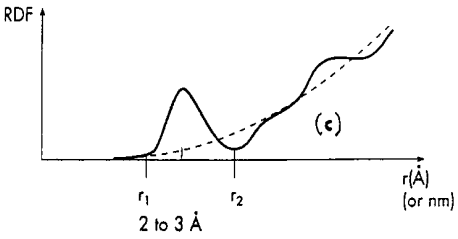

whose integration across peaks yields atomic coordination numbers.

Effect of correlated atomic vibrations at low-r

At short interatomic distances the peaks in PDF(r) are sharper and taller (conserving area $\propto$ coordination number) as compared to the neutron coherence volume's FWHM $\sim$ 60 Å for the D4c diffractometer:

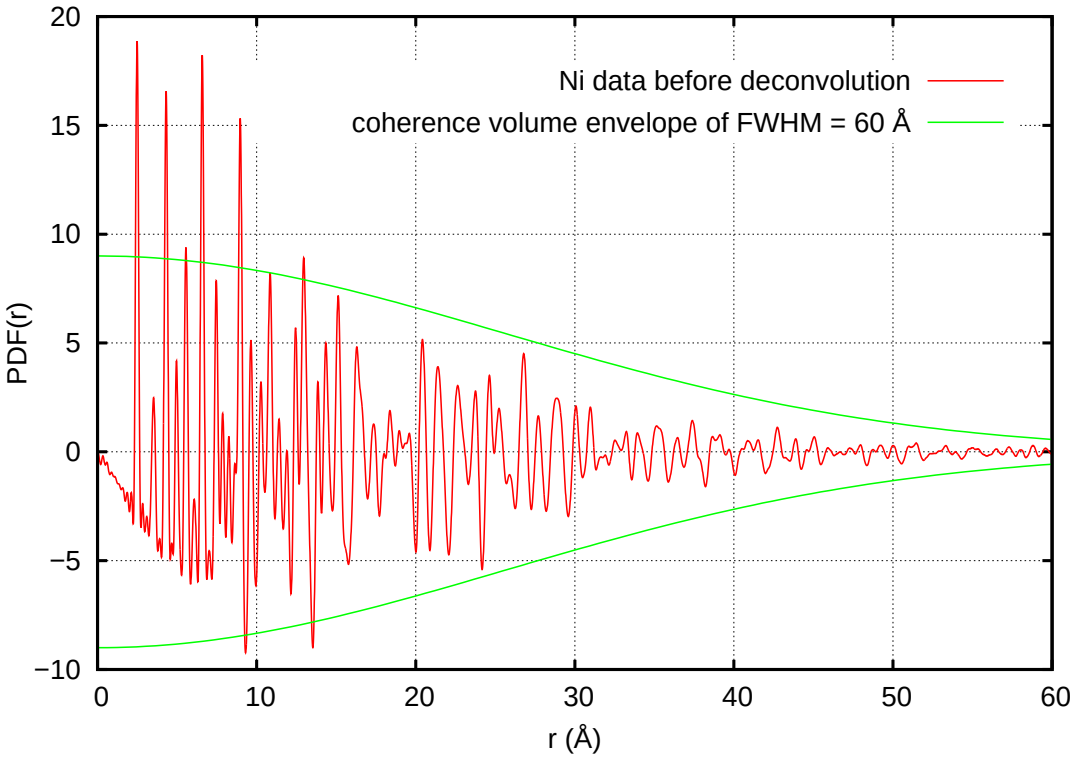

mPDF-analysis
Henry E. Fischer
Diffraction basics
PDF-analysis
PDF examples
UO_2
carbon
mPDF-analysis
mPDF examples
$SrGd_2O_4$
Gd_2O_3
$Gd_2Ir_2O_7$
EuPtGe
$TmMgGaO_4$
$SrNd_2O_4$
mPDF fans
Conclusions
Table of Contents

Vibration modes seen by Rietveld vs PDF-analysis

Whereas Rietveld refinement gives time-averaged distances between atomic pairs, PDF-analysis sees an ensemble-average of quasi-instantaneous atomic positions and relative distances:

Correlated vibrations

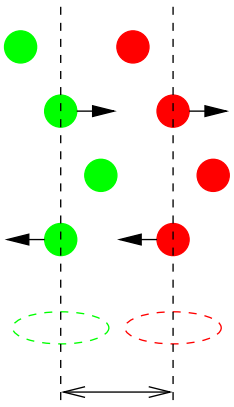

Anti−correlated vibrations

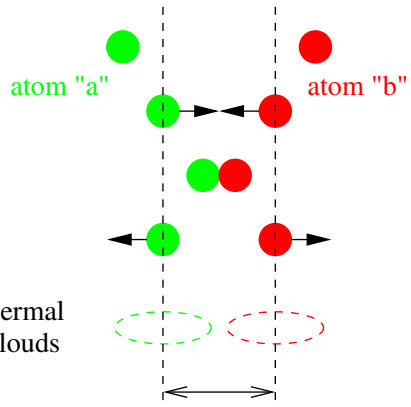

Libration mode

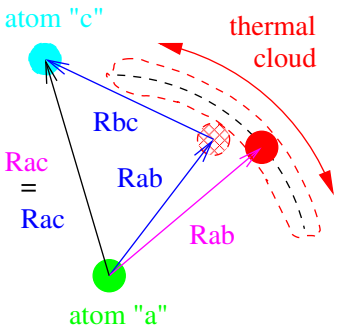

Rietveld−refined Rab = PDF−analysed Rab
for both correlated and anti−correlated vibrations, but Rietveld's time−averaged thermal clouds cannot distinguish between the two cases. PDF(r) will however show a broader peak for the a−b atomic pair in the anti−correlated case.

The time−averaged position of atom b is the barycenter of its banana−shaped thermal cloud, which is closer to atom a than any instantaneous position:

Rab (too short) < Rab (correct)

PDF(r) will show a sharp peak for the a−b and a−c atomic pairs but a very broad peak for b−c.

Atomic PDF(r) examples

mPDF-analysis
Henry E. Fischer
Diffraction basics
PDF-analysis
PDF examples
UO_2
carbon
mPDF-analysis
mPDF examples
$SrGd_2O_4$
Gd_2O_3
$Gd_2Ir_2O_7$
EuPtGe
$TmMgGaO_4$
$SrNd_2O_4$
mPDF fans
Conclusions
Table of Contents

Correlated thermal disorder for O in high-T UO_2?

Increased amplitudes of atomic vibration **u** at higher T lead to broader time-averaged "thermal clouds" of atomic positions that reduce Bragg peak intensities via the Debye-Waller factor $\exp[-\langle(\mathbf{Q}_{hkl}\cdot\mathbf{u})^2\rangle/2]$, which is a Gaussian-like *modulation* in q-space:

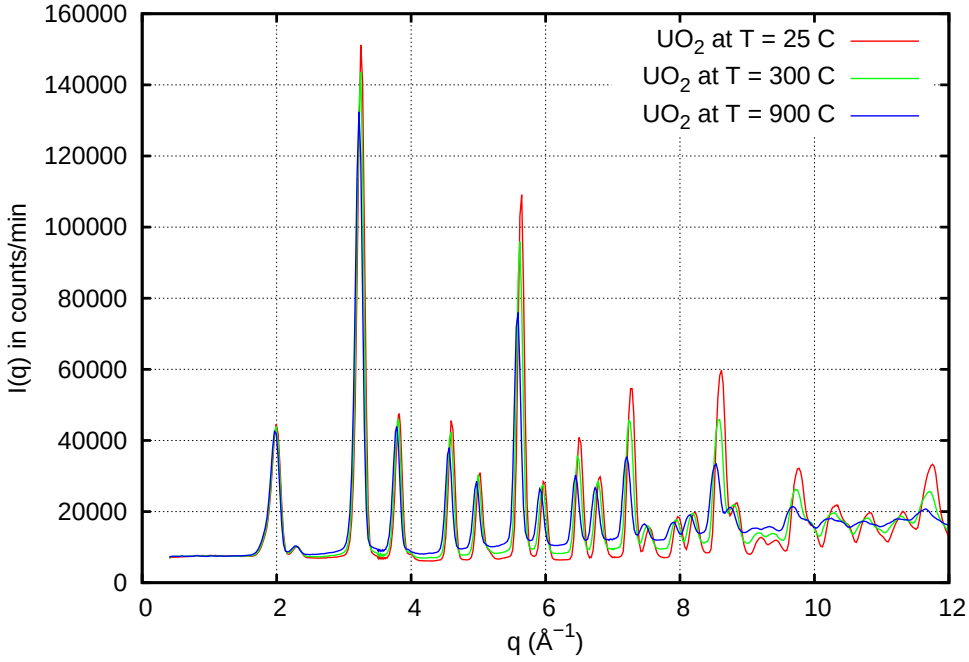

The lost intensity becomes Thermal Diffuse Scattering (TDS).

The Debye-Waller factor in *r*-space

The convolution theorem states that a modulation in *q*-space leads to a convolution in *r*-space (and vice-versa), such that the the D-W factor broadens the peaks in $\mathrm{PDF}(r)$ according to the vibration amplitudes of the corresponding atomic pairs, while preserving the peak areas which are proportional to (generally constant) coordination number:

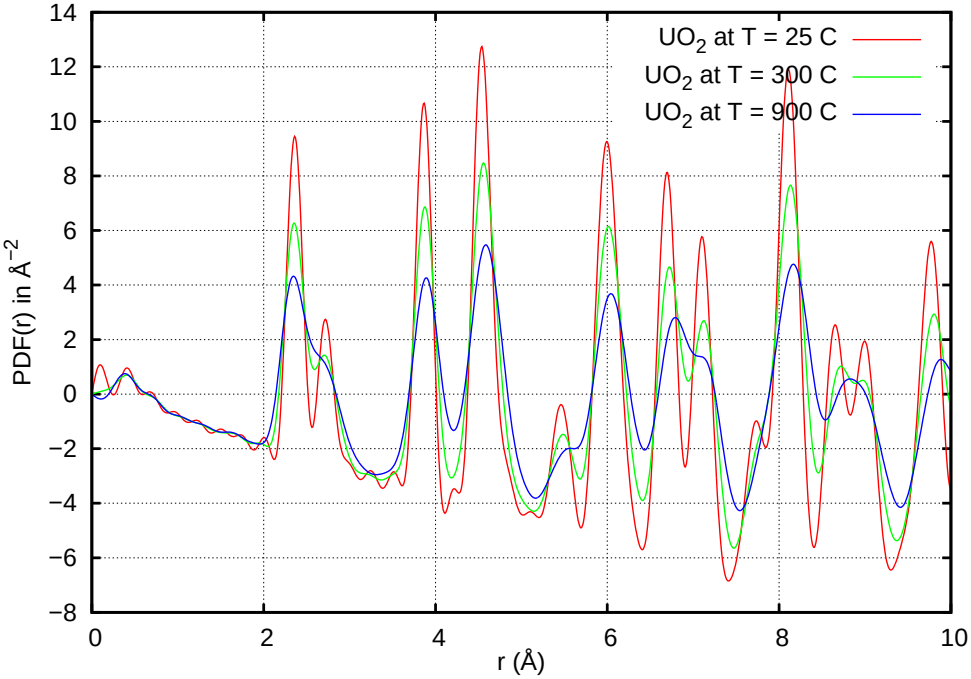

mPDF-analysis
Henry E. Fischer
Diffraction basics
PDF-analysis
PDF examples
UO_2
carbon
mPDF-analysis
mPDF examples
$SrGd_2O_4$
Gd_2O_3
$Gd_2Ir_2O_7$
EuPtGe
$TmMgGaO_4$
$SrNd_2O_4$
mPDF fans
Conclusions
Table of Contents

Dynamic local Pa-3 symmetry in UO_2? (D4@ILL)

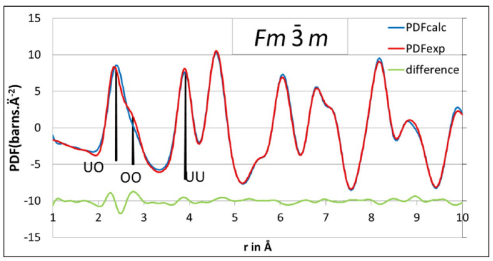

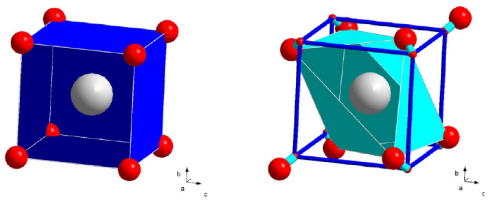

Figure 1. Uranium polyhedron coordination in *Fm*3̄*m* (left) and *Pa*3̄ (right). Uranium and oxygen atoms are colored gray and red, respectively.

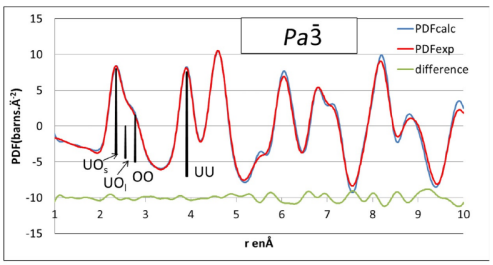

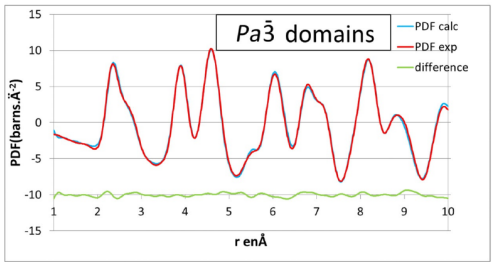

PDF-analysis of UO_2 at 1273 K reveals an asymmetric first-neighbor U-O peak, expected from anharmonic atomic vibrations, that could be explained by *dynamically* correlated O-atom displacements with local Pa-3 symmetry, *i.e.* lower than the space+time averaged Fm-3m symmetry. In any case, the O vibration amplitudes are quite large.

L. Desgranges, et al, *Inorg. Chem.* **56** *(2017) 321.*

R.I. Palomares, et al, *Phys. Rev. Mat.* **3** *(2019) 053611.*

PDF analysis at D4@ILL: different forms of carbon

Q-space:

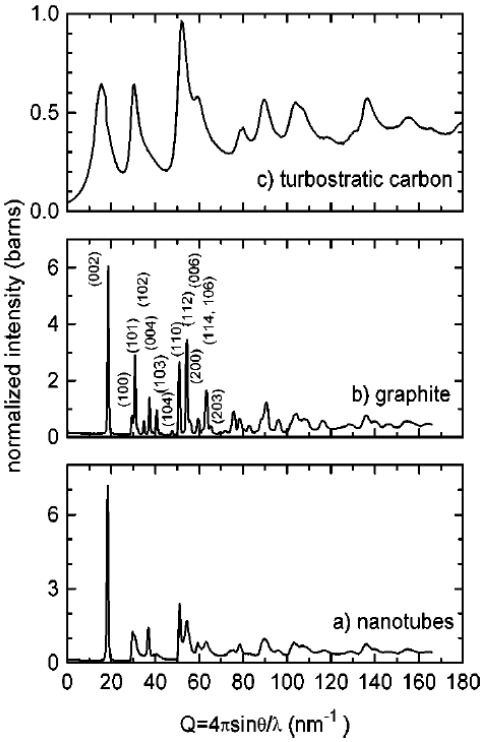

R-space:

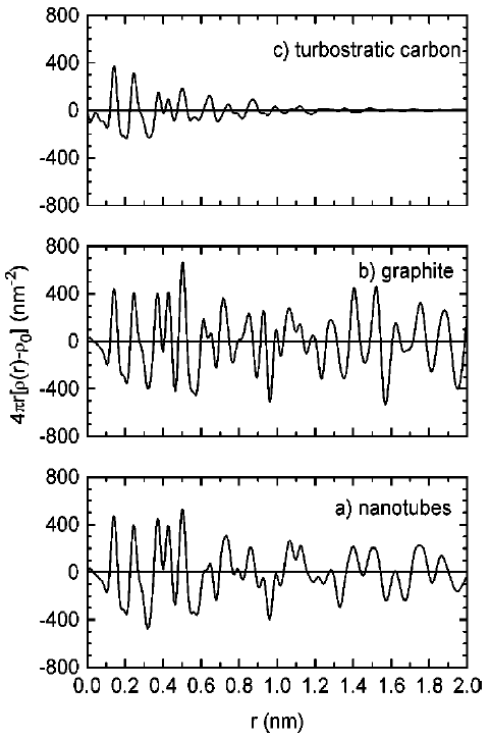

A. Burian, J.C. Dore, H.E. Fischer and J. Sloan, Phys. Rev. B **59** *(1999) 1665–8 (***60** *citations).*

mPDF-analysis
Henry E. Fischer
Diffraction basics
PDF-analysis
PDF examples
UO_2
carbon
mPDF-analysis
mPDF examples
$SrGd_2O_4$
Gd_2O_3
$Gd_2Ir_2O_7$
EuPtGe
$TmMgGaO_4$
$SrNd_2O_4$
mPDF fans
Conclusions
Table of Contents

Atomic PDF-analysis: FT of a powder diffractogram

Disordered, nano-structured or reduced-dimensional crystals often lack sufficient long-range order to produce sharp diffraction peaks. It is then advantageous to sacrifice q-space resolution by using short wavelengths to provide a high $q_{\max}$ and thus better r-space resolution $\Delta r = 3.79/q_{\max}$ after Fourier Transform (FT) of the diffraction pattern $d\sigma/d\Omega - \text{self\_scattering}$.

The resulting Pair-Distribution Function PDF(r) is the distribution of relative interatomic distances with respect to an average atom at the origin (*i.e.* an ensemble of quasi-instantaneous local structures $\neq$ the time+space averaged structure from Rietveld).

q-space resolution Δq leads to an envelope that modulates and limits the spatial extent of the PDF(r) via $r_{\max} = (5.55/2)/\Delta q$.

NB: The PDF(r) is not the output of structural refinement, and is therefore a *model-independent* result that can of course then be used as input for structural modelling/simulation in r-space.

Magnetic PDF-analysis

mPDF-analysis
Henry E. Fischer
Diffraction basics
PDF-analysis
PDF examples
UO_2
carbon
mPDF-analysis
mPDF examples
$SrGd_2O_4$
Gd_2O_3
$Gd_2Ir_2O_7$
EuPtGe
$TmMgGaO_4$
$SrNd_2O_4$
mPDF fans
Conclusions
Table of Contents

Generalizing to magnetic total scattering

Recall the total (nuclear) differential scattering cross-section per atom:

$$\frac{1}{N}\frac{d\sigma}{d\Omega} = \overline{b}^2\,[S(Q)-1] + \overline{b^2}$$

which comprises a "distinct" term (interference between different atoms) and a "self" term $\overline{b^2}$ (self-interference from individual atoms). As first derived by Blech and Averbach (1964), the total *magnetic* differential scattering cross-section per atom for a system of N identical spins is:

$$\left.\frac{1}{N}\frac{d\sigma}{d\Omega}\right|_{\mathrm{m}} = p^2\mu^2 f^2(Q)$$

$$\cdot\left\{\frac{2}{3} + \frac{1}{N}\sum_{i\neq j}\left[A_{ij}\frac{\sin(Qr_{ij})}{Qr_{ij}} + B_{ij}\left(\frac{\sin(Qr_{ij})}{(Qr_{ij})^3} - \frac{\cos(Qr_{ij})}{(Qr_{ij})^2}\right)\right]\right\},$$

where μ is the atomic magnetic moment in units of Bohr magnetons μ_{B}, $p = \gamma_n r_e/2 = 2.696$ fm, $f(Q)$ is the magnetic form factor with $f(0) = 1$, and A_{ij} and B_{ij} are spin-spin orientational correlation functions for spin components respectively perpendicular (*i.e.* transverse) or parallel (*i.e.* longitudinal/collinear) to the interspin vector $\mathbf{r}_{ij} = \mathbf{r}_j - \mathbf{r}_i$.

Generalizing to magnetic total scattering

Now define the neutron magnetic scattering length (unpolarized case):

$$b_{\rm m}(Q) \stackrel{\rm def}{=} \sqrt{\frac{2}{3}}\, p\,\mu\, f(Q)$$

The magnetic self-scattering per atom of the magnetic species is then:

$$\left.\frac{d\sigma}{d\Omega}\right|_{\rm m,self} = b_{\rm m}^2(Q) = \frac{2}{3}p^2\mu^2 f^2(Q)$$

and corresponds to the magnetic diffraction intensity per spin in the absence of orientational correlations between neighboring spins. Such a sample with zero spin-spin correlations is simply in the paramagnetic state. Since we are interested precisely in the correlations between magnetic spins, we subtract the magnetic self-scattering from the total magnetic differential scattering cross-section to obtain:

$$I_{\rm m}(Q) \stackrel{\rm def}{=} \frac{1}{N}\left.\frac{d\sigma}{d\Omega}\right|_{\rm m} - b_{\rm m}^2(Q)$$

$$= p^2\mu^2 f^2(Q)\cdot\frac{1}{N}\sum_{i\neq j}\left[A_{ij}\frac{\sin(Qr_{ij})}{Qr_{ij}} + B_{ij}\left(\frac{\sin(Qr_{ij})}{(Qr_{ij})^3} - \frac{\cos(Qr_{ij})}{(Qr_{ij})^2}\right)\right].$$

The magnetic Pair-Distribution Function mPDF(r)

Recall that the atomic PDF(r) is obtained by Fourier transform of $S(Q)-1$, namely the diffraction intensity $d\sigma/d\Omega$ per atom after subtraction of the self-scattering $\overline{b^2}$ and division by $\overline{b}^2$:

$$\mathrm{PDF}(r) = \frac{2}{\pi}\int_0^\infty Q\,[S(Q)-1]\,\sin(Qr)\,dQ = \frac{1}{N}\sum_{i\neq j}^{N}\frac{1}{r}\delta(r-r_{ij})\,.$$

Likewise the normalized self-scattering-subtracted magnetic diffraction intensity $I_{\rm m}(Q)$ can also be analytically Fourier transformed (first done by B.A. Frandsen, *et al* in 2014) to produce the *model-independent* magnetic Pair-Distribution Function or mPDF(r):

$$\mathrm{mPDF}(r) \stackrel{\rm def}{=} \frac{2}{\pi}\int_0^\infty Q\,\frac{I_{\rm m}(Q)}{\frac{2}{3}p^2\mu^2}\,\sin(Qr)\,dQ$$

$$\approx \frac{3}{2}\cdot\frac{1}{N}\sum_{i\neq j}\left[\frac{A_{ij}}{r}\tilde{\delta}(r-r_{ij}) + B_{ij}\frac{r}{r_{ij}^3}[1-\tilde{\Theta}(r-r_{ij})]\right],$$

that represents both static and dynamic local spin-spin correlations, where the delta-function $\tilde{\delta}(r-r_{ij})$ and the Heaviside step function $\tilde{\Theta}(r-r_{ij})$ have been broadened by $\mathrm{FWHM_R} \approx 4\ln(4)/\mathrm{FWHM}_{f^2(Q)}$ since we chose for experimental reasons not to divide $I_{\rm m}(Q)$ by $f^2(Q)$.

Generalities about magnetic PDF-analysis

For non-polarized neutron diffraction from 1 pair of F or AF magnetic spins, $f(r) = \mathrm{mPDF}(r)$ clearly indicates whether the spins' orientation is transverse (showing a strong peak) or longitudinal/collinear (showing a strong slope at low-r) with respect to the interspin vector $\mathbf{r}_{ij} = \mathbf{r}_j - \mathbf{r}_i$.

ferromagnetic:

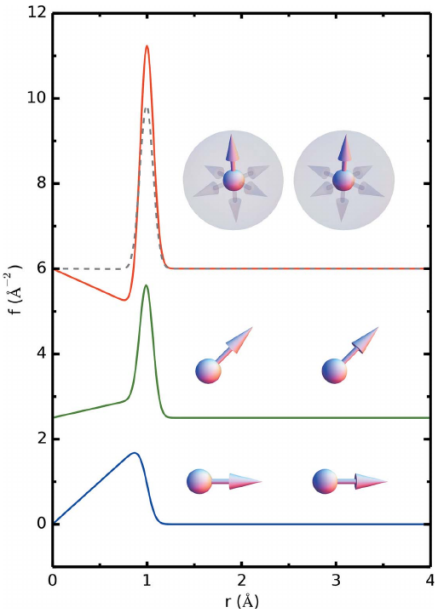

anti-ferromagnetic:

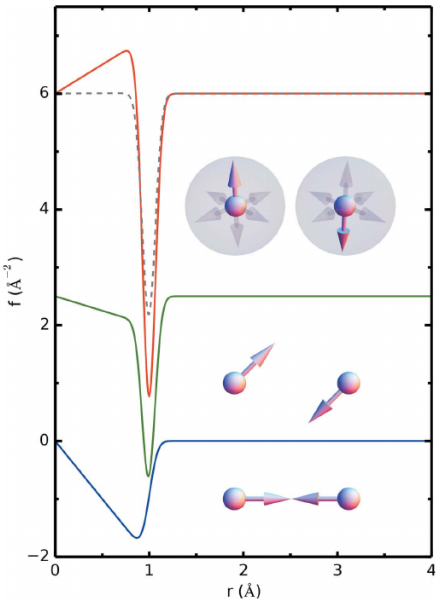

B.A. Frandsen, et al*, Acta. Cryst. A* **70** *(2014) 3–12.*

Generalities about magnetic PDF-analysis (cont'd)

In 1D and 3D systems, transverse versus collinear magnetic structures for F/AF can generally be distinguished respectively by positive/negative peaks versus positive/negative low-r slopes in the mPDF(r), except in the case of rotational invariance imposed by cubic lattice symmetry.

AF 1-D chain of spins:

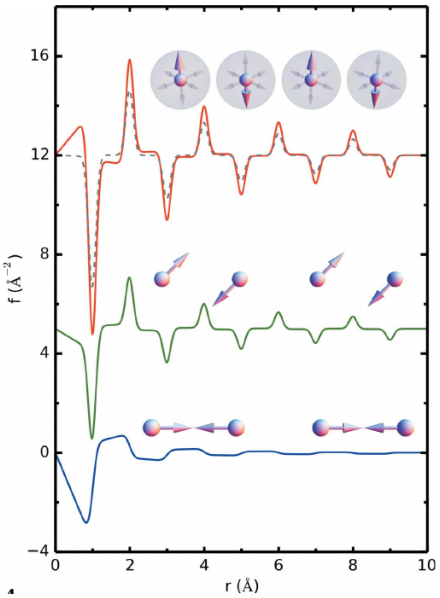

AF 3-D cubic structure:

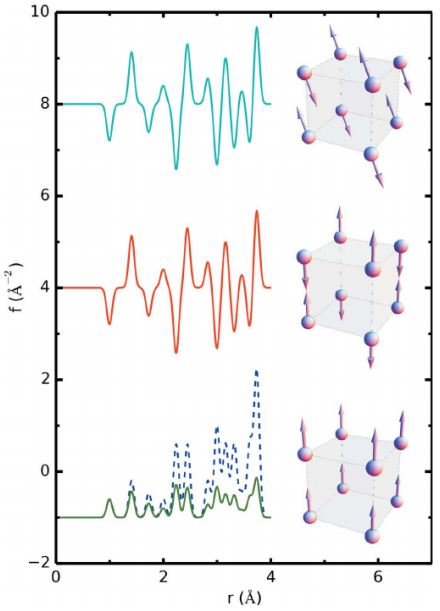

B.A. Frandsen, et al*, Acta. Cryst. A* **70** *(2014) 3–12.*

Modeling techniques for Magnetic PDF-analysis:

Small box modeling (*e.g.* the diffpy.mpdf module for DiffPy-CMI) :

- R-space based *refinement* of spin orientations and perhaps other parameters to fit the measured mPDF(r) – similar to PDFgui, MolPDF.
- Small number of spins, perhaps only one magnetic unit cell.
- Qmax and Qmin are inputed to simulate experimental conditions.
- Additional parameters to dampen and/or broaden the mPDF, simulating the effects of thermal motion and instrumental resolution.

$\Rightarrow$ Runs fast, fits directly the mPDF(r), but susceptible to mixing instrumention effects with structural features.

Large box modeling (*e.g.* Spinvert, RMCprofile) :

- Q-space based *Reverse Monte Carlo* simulation of spin orientations to fit the measured magnetic diffuse scattering $I_m(Q)$.
- Large number (thousands) of spins, corresponding to the dimensions of the neutron coherence volume.
- The fit to $I_m(Q)$ is FT-ed to produce the simulated mPDF(r).

$\Rightarrow$ Accurately treats instrumention effects, can smooth out noisy data, permits sampling of spin-spin correlation functions, but runs more slowly and can be susceptible to maximum-entropy effects and local minima.

mPDF-analysis
Henry E. Fischer
Diffraction basics
PDF-analysis
PDF examples
UO_2
carbon
mPDF-analysis
mPDF examples
$SrGd_2O_4$
Gd_2O_3
$Gd_2Ir_2O_7$
EuPtGe
$TmMgGaO_4$
$SrNd_2O_4$
mPDF fans
Conclusions
Table of Contents

Magnetic PDF(r) examples

Nuclear structure of $SrRE_2O_4$ (*Pnma*, No. 62)

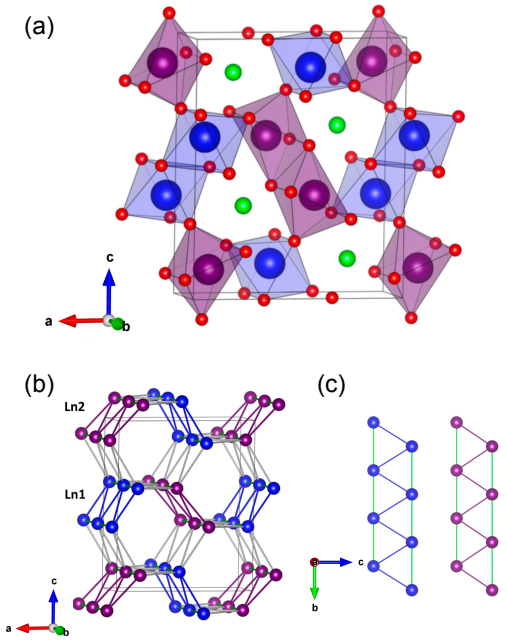

(a) The orthorhombic unit cell of the $SrRE_2O_4$ structure. The magnetic RE ions occupy two distinct 4*c* Wyckoff sites having octahedral O-coordination and forming around Sr atoms distorted hexagons. (b) The *distorted honeycomb structure* of the magnetic ions manifests along the *b*-axis two types of *zig-zag ladders* (shown in (c)) containing triangles that induce a large degree of *geometrical frustration* due to the NN anti-ferromagnetic exchange.

The two slightly different crystallographic environments of the RE ions at two distinct 4*c* Wyckoff sites $(x, \frac{1}{4}, z)$ leads to different magnetic ordering in the case of strong CEF effects. Rietveld results (D20@ILL) show that $SrGd_2O_4$ exhibits *longitudinal F* order along each 1D chain but AF correlations between the two chains of a given zig-zag ladder.

mPDF-analysis
Henry E. Fischer
Diffraction basics
PDF-analysis
PDF examples
UO_2
carbon
mPDF-analysis
mPDF examples
$SrGd_2O_4$
Gd_2O_3
$Gd_2Ir_2O_7$
EuPtGe
$TmMgGaO_4$
$SrNd_2O_4$
mPDF fans
Conclusions
Table of Contents

Diffraction data for $SrGd_2O_4$ (D4c@ILL, $\lambda = 0.5$ Å)

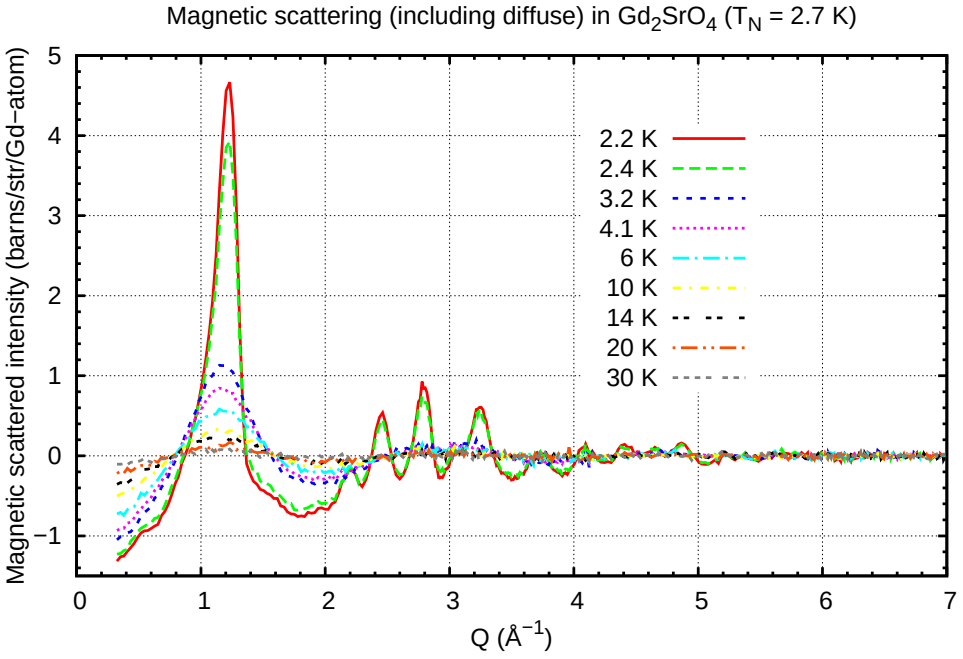

After subtraction of a 50 K "paramagnetic baseline", representing the *Q*-dependent magnetic self-scattering, and normalization via vanadium to an absolute diffraction intensity scale as $d\sigma/d\Omega$.

mPDF(r) data for $SrGd_2O_4$ (D4c@ILL $\lambda = 0.5$ Å)

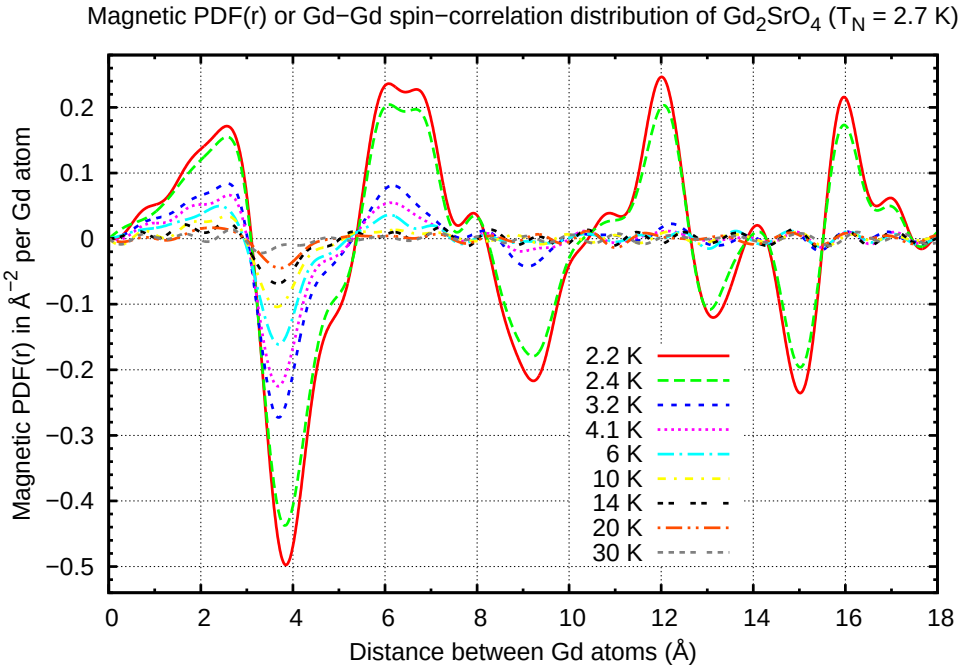

Fourier transform for $Q_{\max} = 7$ Å^{-1} after dividing by the magnetic self-scattering $\frac{2}{3}p^2\mu^2$ (*i.e.* sans form factor squared $f^2(Q)$).

mPDF-analysis
Henry E. Fischer
Diffraction basics
PDF-analysis
PDF examples
UO_2
carbon
mPDF-analysis
mPDF examples
$SrGd_2O_4$
Gd_2O_3
$Gd_2Ir_2O_7$
EuPtGe
$TmMgGaO_4$
$SrNd_2O_4$
mPDF fans
Conclusions
Table of Contents

Reverse Monte Carlo simulations using SPINVERT

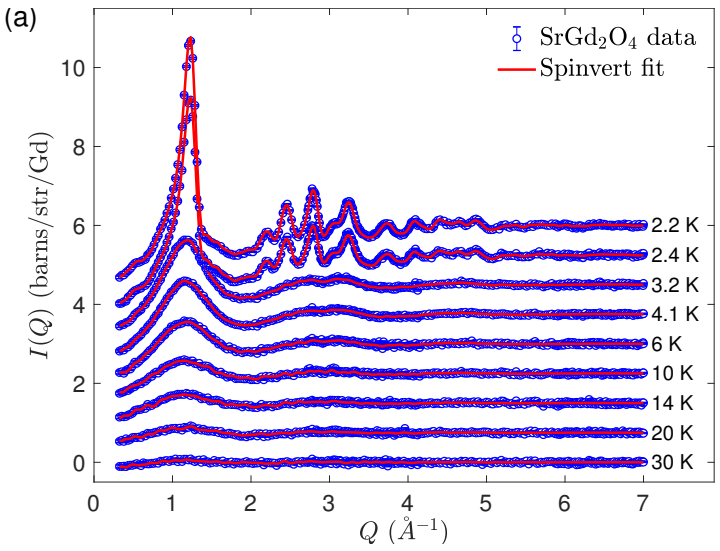

RMC simulations using SPINVERT* fit well the intensity-normalized, 50K-subtracted magnetic diffraction data in Q-space ($T_N = 2.7$ K). Ising spins $\parallel$ b are used in a simulation box of 9 x 27 x 9 unit cells that corresponds to the $\sim$ 60 Å spherical neutron coherence volume, and thus to the Q-space resolution, of the D4c neutron diffractometer.

J.A.M. Paddison, et al*, J. Phys.: Condens. Matter* **25** *(2013) 454220.*

r-dependence of the spin-spin correlations

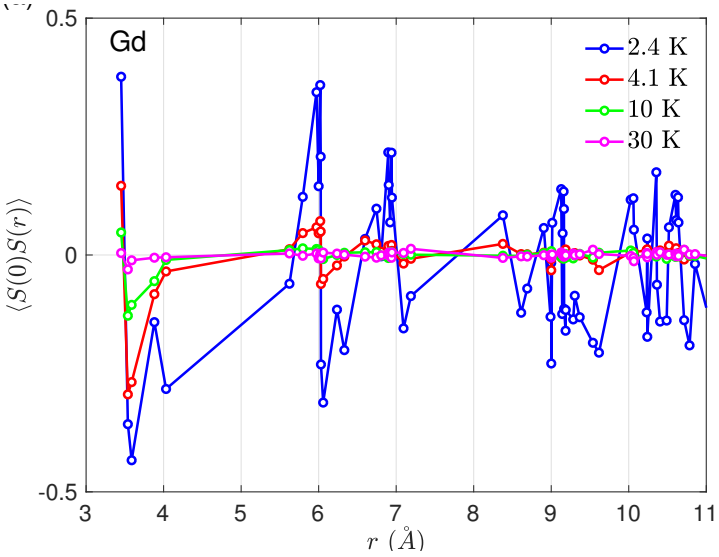

The simple dot-product spin-spin correlation function $\langle \mathbf{S}(0) \cdot \mathbf{S}(r) \rangle$, obtained from the RMC fits, gives the ensemble-averaged alignment between two identifiable spins at a given instant, as separated by the interspin distance r, independent of the direction of the interspin vector $\mathbf{r}_{ij} = \mathbf{r}_j - \mathbf{r}_i$. Clearly observable well above T_N are some short-range *dynamic* spin-spin correlations. Strong correlations at large r indicate long-range *static* correlations (*i.e.* magnetic order) that set in below T_N.

mPDF-analysis
Henry E. Fischer
Diffraction basics
PDF-analysis
PDF examples
UO_2
carbon
mPDF-analysis
mPDF examples
$SrGd_2O_4$
Gd_2O_3
$Gd_2Ir_2O_7$
EuPtGe
$TmMgGaO_4$
$SrNd_2O_4$
mPDF fans
Conclusions
Table of Contents

T-dependence of the spin-spin correlations

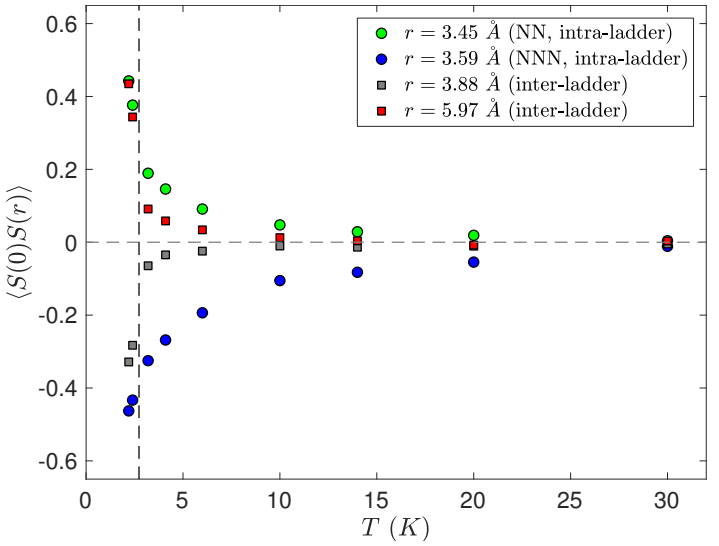

$\langle \mathbf{S}(0) \cdot \mathbf{S}(r) \rangle$ can be obtained from the RMC fits for selected intra-chain, inter-chain (*i.e.* intra-ladder) & inter-ladder distances as a function of T. Strong *intra*-ladder correlations (circles) are observed far above T_N (vertical dashed line). *Inter*-ladder correlations (squares) become important only a few K above T_N. All spin-spin correlations are increasingly dynamic as $T > T_N$, and static as $T < T_N$ (dashed line).

mPDF(r) derived analytically and from RMC fits

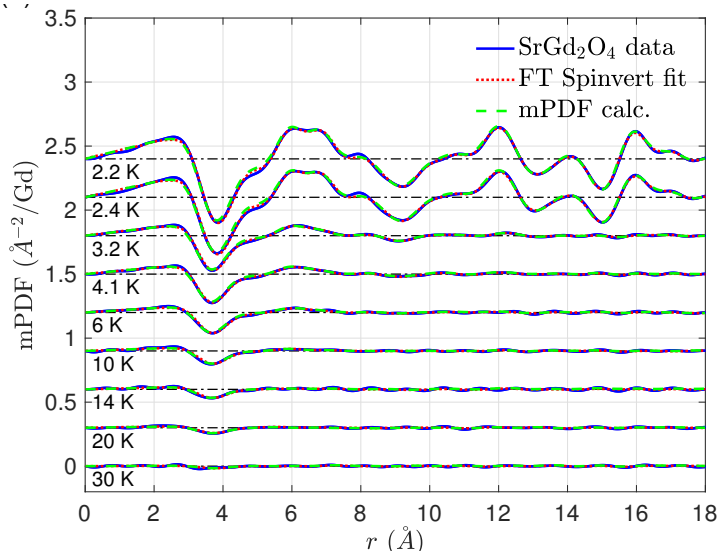

The analytical calculations of the mPDF(r) make use of the spin configurations generated by Spinvert, from which are calculated the A_{ij} and B_{ij} spin-spin orientational correlation functions. The strong positive low-r slope confirms the longitudinal F-correlations along 1D chains. The broad negative peak shows the AF correlations between both inter-chain ($r \sim 3.6$ Å) and inter-ladder ($r \sim 3.9$ Å) spins. The positive ~ 6 Å peak indicates ferro NNN-correlations within a hexagon.

D4c and Spinvert results for Gd_2O_3 (monoclinic)

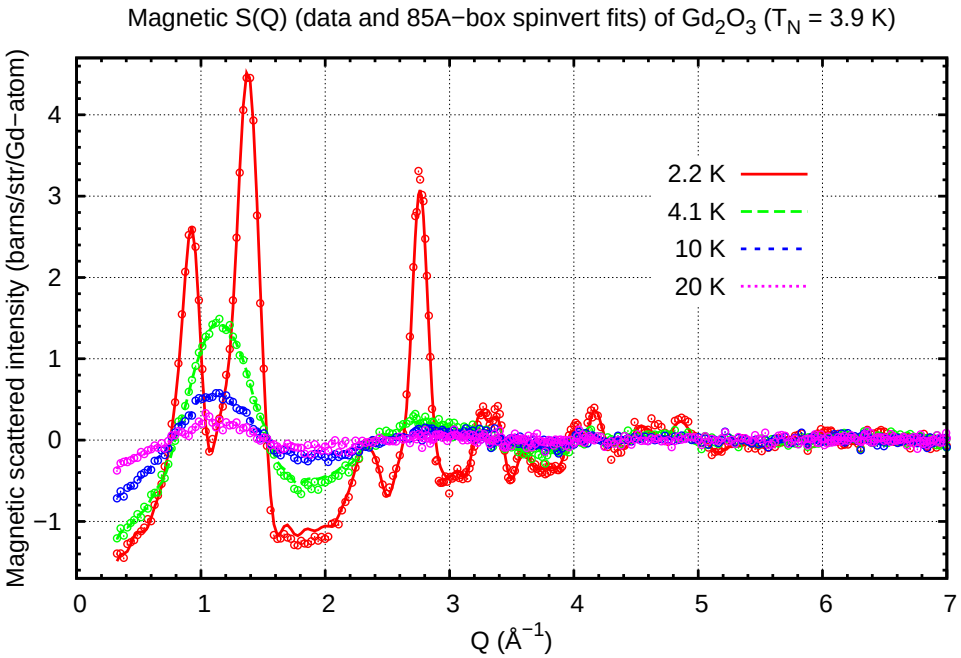

Some quick measurements of magnetic diffraction intensity for the "impurity phase" Gd_2O_3 produced some intriguing results. (Here shown after subtraction of a 50 K "paramagnetic baseline").

Possible metastable spin configurations above T_N?

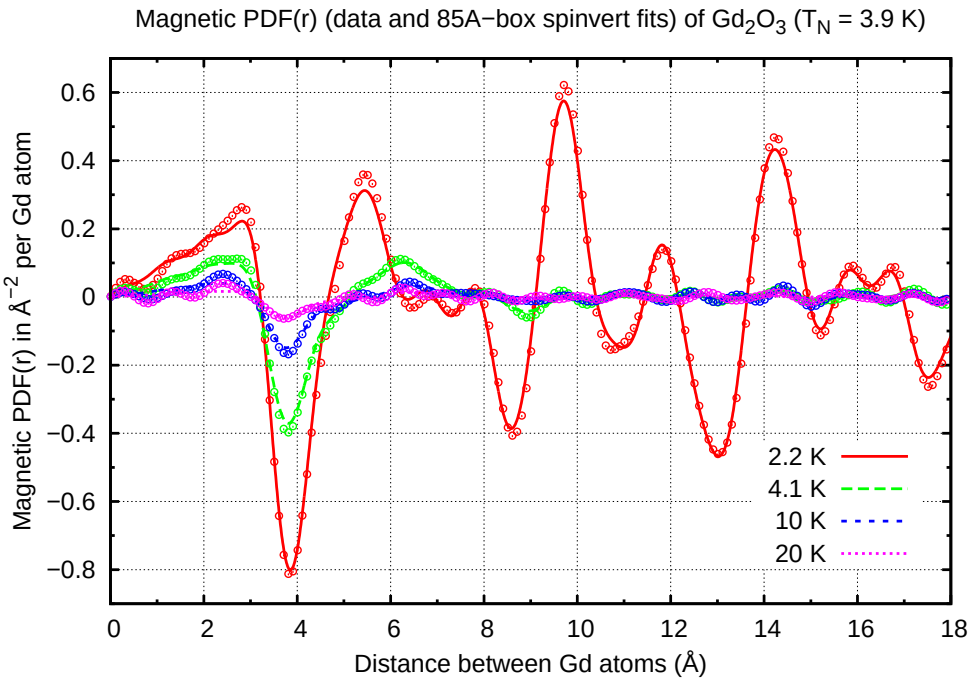

The PDF(r) from the 3D-constrained Spinvert RMC fits in Q-space reproduce the anomalous features at $r = 6$ Å and $r = 9$ Å for $T = 4.1$ K (green curve), corresponding to inter-spin distances that do not show significant correlations in the ordered magnetic structure below T_N.

mPDF-analysis
Henry E. Fischer
Diffraction basics
PDF-analysis
PDF examples
UO_2
carbon
mPDF-analysis
mPDF examples
$SrGd_2O_4$
Gd_2O_3
$Gd_2Ir_2O_7$
EuPtGe
$TmMgGaO_4$
$SrNd_2O_4$
mPDF fans
Conclusions
Table of Contents

Curious liquid-like spin correlations well above T_N?

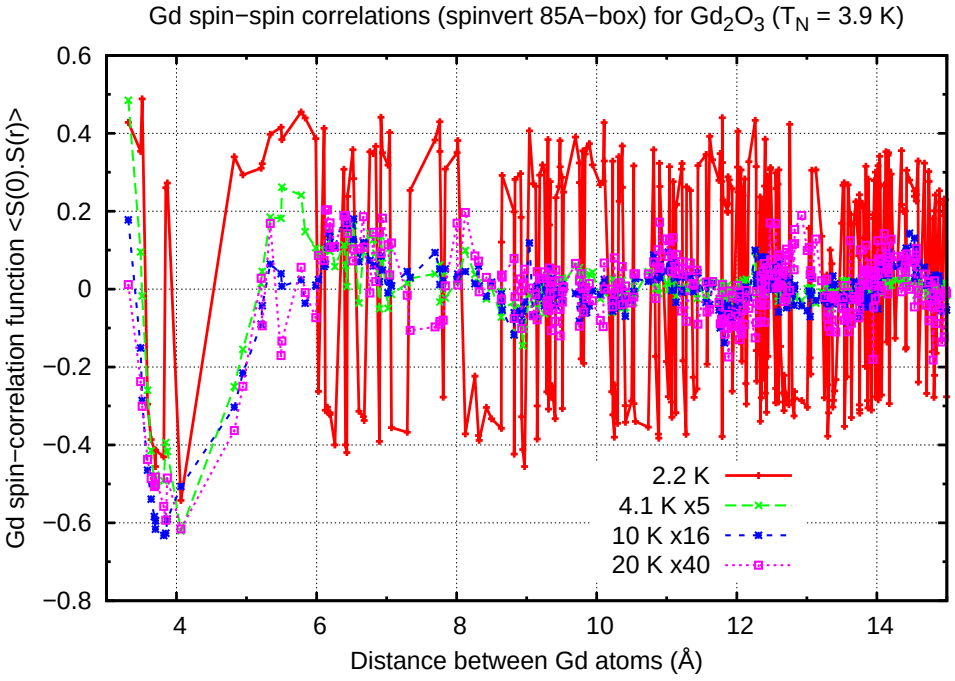

The dot-product spin-spin correlation function, which neglects the orientation of the interspin vector, displays liquid-like oscillations at high-r of diminishing amplitude as $T > T_N$. Analogous composition correlations are seen at high-r in atomic PDFs of *e.g.* molten $ZnCl_2$.

Magnetic PDF-analysis of the pyrochlore $Gd_2Ir_2O_7$

Total magnetic scattering in *q*-space (c) and *r*-space (d, 3K-50K):

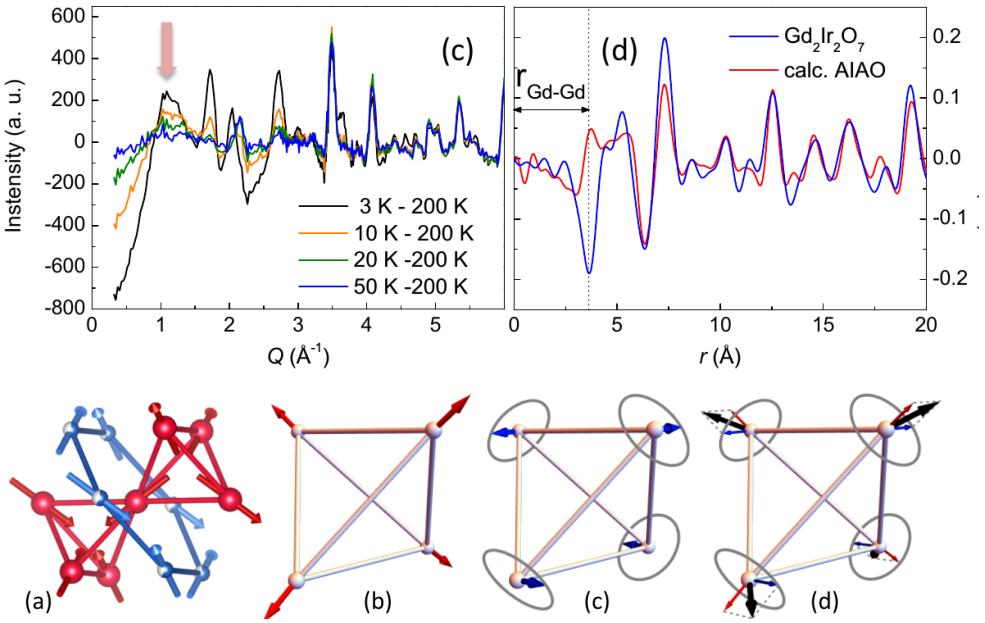

The mPDF(r) results from D4 allowed to conclude that the Gd magnetic structure at low-T in this geometrically frustrated material (d) manifests a coexistence of AIAO (a,b) and Palmer-Chalker (c) configurations.
E. Lefrançois, et al*, Phys. Rev. B* **99** *(2019) 060401(R).*

mPDF-analysis
Henry E. Fischer
Diffraction basics
PDF-analysis
PDF examples
UO_2
carbon
mPDF-analysis
mPDF examples
$SrGd_2O_4$
Gd_2O_3
$Gd_2Ir_2O_7$
EuPtGe
$TmMgGaO_4$
$SrNd_2O_4$
mPDF fans
Conclusions
Table of Contents

F vs AF correlations in EuPtGe (cubic $P2_13$, # 198)

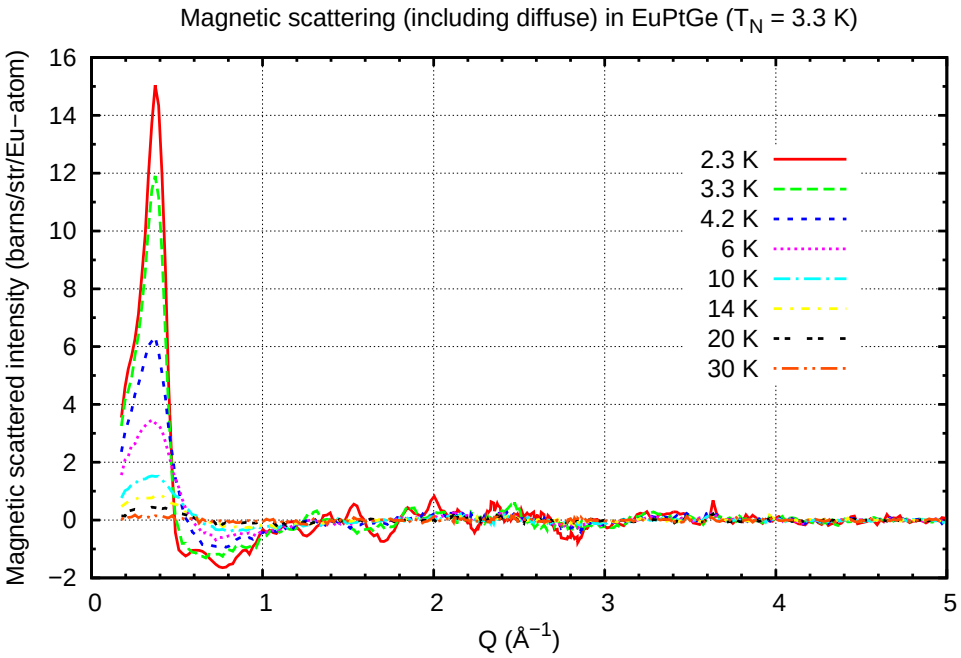

Puzzle : First-order magnetic transition to AF at $T_N = 3.3$ K but $\Theta_{CW} > 0$ from high-T susceptibility, hence predominantly F interactions. Specific heat shows spin entropy is recovered only at several times T_N, implying strongly correlated spin fluctuations.

mPDF(r) data for EuPtGe (D4c@ILL, $\lambda = 0.7$ Å)

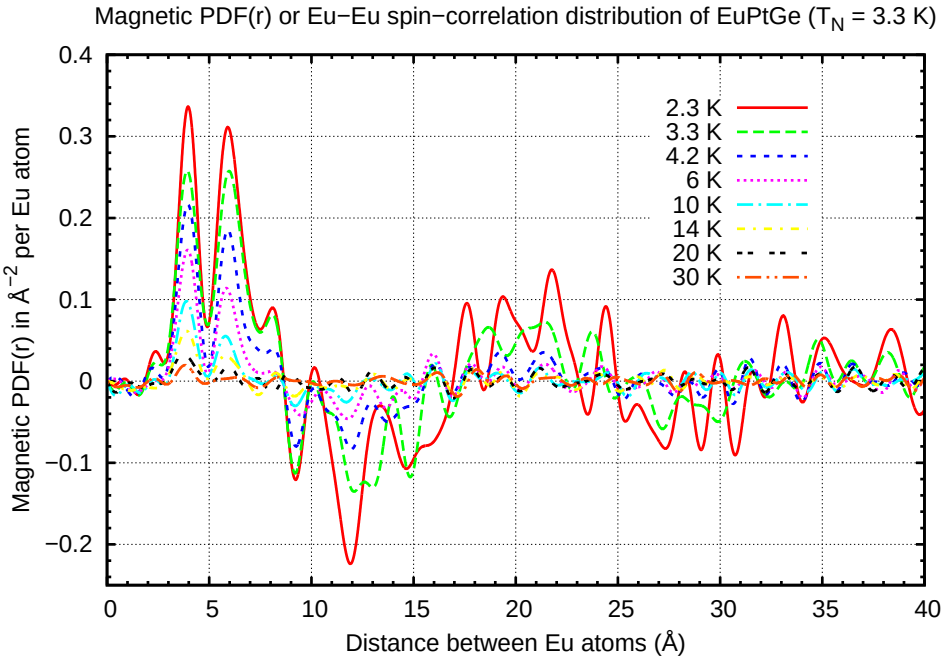

Quick semi-quantitative analysis of the mPDF(r) suggests a helical structure ($\sim$ 17 Å period) of Eu^{2+} spins correlated F within a given plane $\perp$ **k**, producing zero net F-ordered moment after n planes.
NB: Low-T helical phase found in EuPt**Si** from ND/single-crystal:
K. Kaneko, et al*, J. Phys. Soc. Jpn.* **88** *(2019) 013702.*

mPDF-analysis
Henry E. Fischer
Diffraction basics
PDF-analysis
PDF examples
UO_2
carbon
mPDF-analysis
mPDF examples
$SrGd_2O_4$
Gd_2O_3
$Gd_2Ir_2O_7$
EuPtGe
$TmMgGaO_4$
$SrNd_2O_4$
mPDF fans
Conclusions
Table of Contents

Structure of $TmMgGaO_4$ (trigonal $R\bar{3}m$, No. 166)

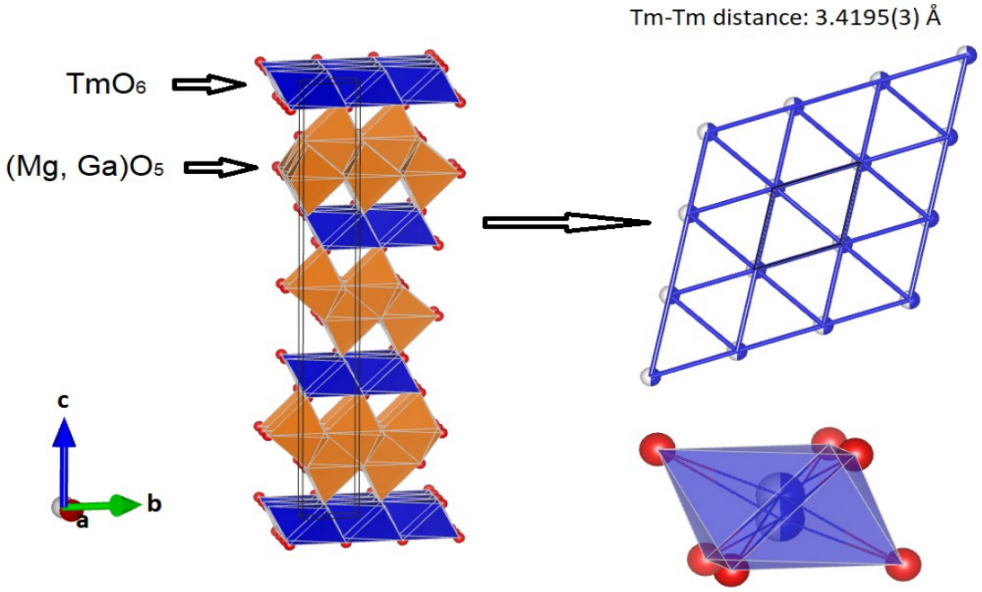

The Tm^{3+} ions form a quasi-2D triangular lattice within a sheet of distorted TmO_6 coordination polyhedra.

F.A. Cevallos, et al*, Mat. Res. Bull.* **105** *(2018) 154.*

$TmMgGaO_4$ diffraction data (D4c@ILL, $\lambda = 0.5$ Å)

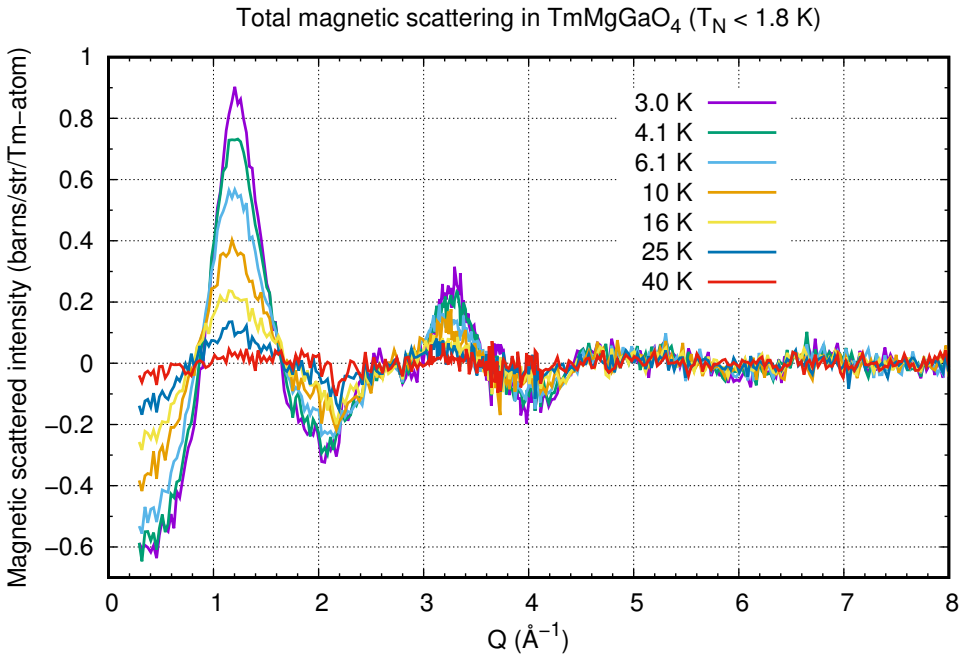

After subtraction of a 50 K "paramagnetic baseline", representing the Q-dependent magnetic self-scattering, and normalization via vanadium to an absolute diffraction intensity scale as $d\sigma/d\Omega$.

mPDF-analysis
Henry E. Fischer
Diffraction basics
PDF-analysis
PDF examples
UO2
carbon
mPDF-analysis
mPDF examples
SrGd2O4
Gd2O3
Gd2Ir2O7
EuPtGe
TmMgGaO4
SrNd2O4
mPDF fans
Conclusions
Table of Contents

mPDF(r) data for $TmMgGaO_4$ (D4c@ILL $\lambda = 0.5$ Å)

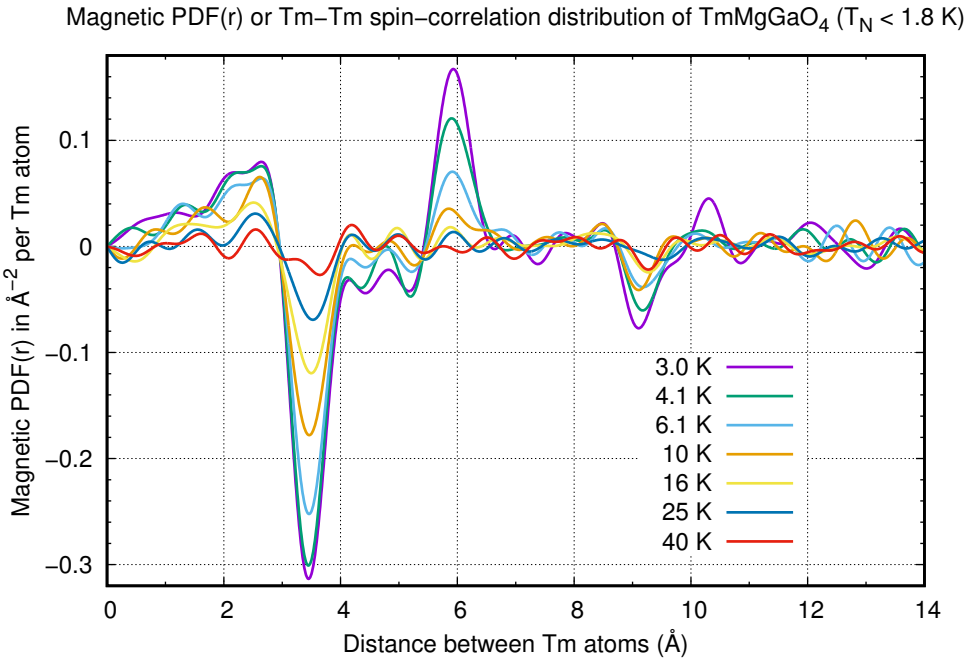

Fourier transform for $Q_{\max} = 8$ Å^{-1} after dividing by the magnetic self-scattering $\frac{2}{3}p^2\mu^2$ (*i.e.* sans form factor squared $f^2(Q)$). Since $T > T_N$, this mPDF(r) represents *dynamic* spin-spin correlations.

Spinvert mPDF(r) results for $TmMgGaO_4$ (60 Å box)

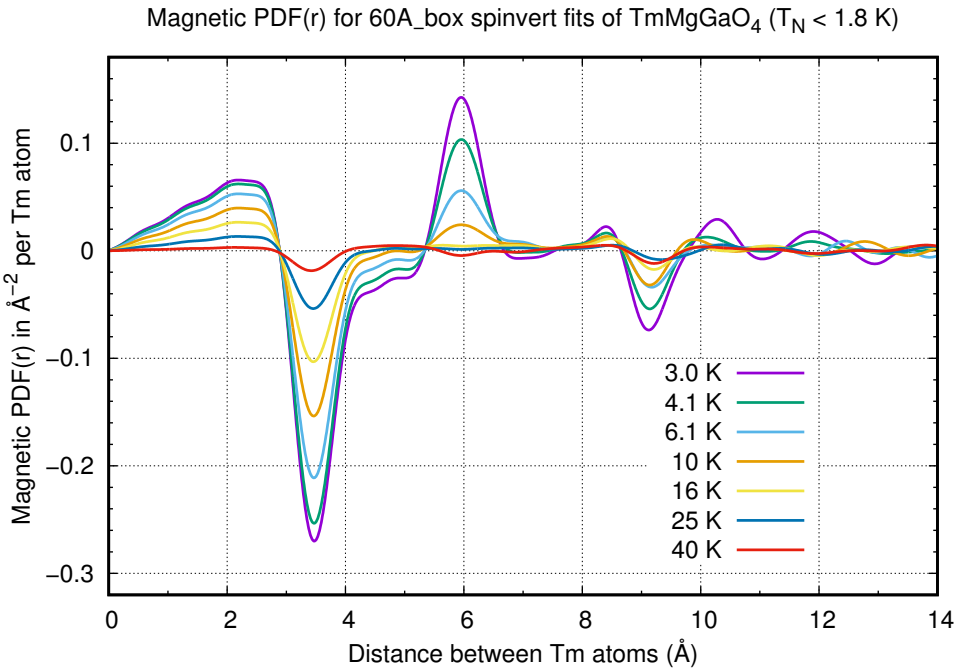

A Fourier transform for $Q_{max} = 8$ Å^{-1} of the Spinvert fit to the Q-space data clearly helps to clean up the statistical noise.

mPDF-analysis
Henry E. Fischer
Diffraction basics
PDF-analysis
PDF examples
UO_2
carbon
mPDF-analysis
mPDF examples
$SrGd_2O_4$
Gd_2O_3
$Gd_2Ir_2O_7$
EuPtGe
$TmMgGaO_4$
$SrNd_2O_4$
mPDF fans
Conclusions
Table of Contents

Spin-spin correlations for $TmMgGaO_4$ (Spinvert)

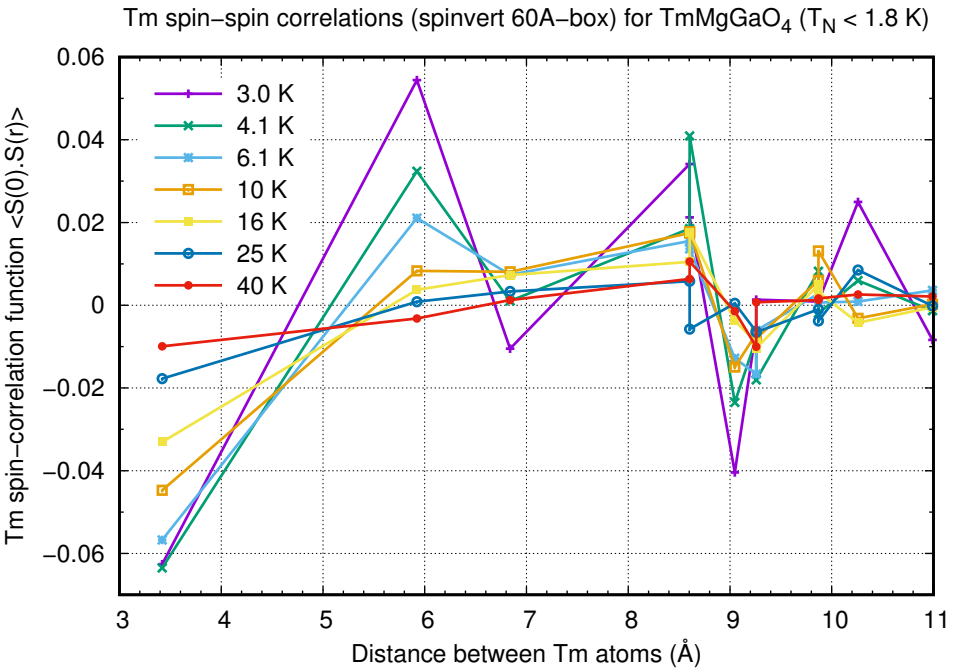

The Tm^{3+} are treated as Heisenberg spins in a 3-D 60 Å box, *i.e.* taking into account spin correlations between triangular lattice layers.

2-D small-box modeling of spins in $TmMgGaO_4$

2D Ising model refinements (spins along c axis); 3 K data

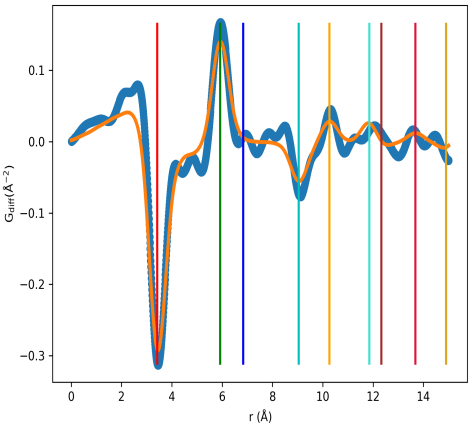

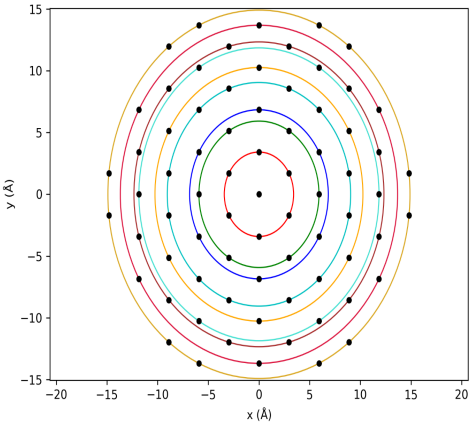

Colored vertical lines correspond to the 2D coordination shells shown to the right.

Note that a 3D model with Heisenberg-type spins provides a slightly better fit, but the spins naturally converge to an approximately Ising configuration with weak inter-layer correlation.

1st NN: Net Antiferromagnetic
2nd NN: Net Ferro
3rd NN: Correlations average to zero
4th NN: Net AF
5th: NN: Net Ferro

The 2-D assumption of negligeable coupling between Tm layers facilitates the testing of theoretical models (work in progress!).

mPDF-analysis
Henry E. Fischer
Diffraction basics
PDF-analysis
PDF examples
UO_2
carbon
mPDF-analysis
mPDF examples
$SrGd_2O_4$
Gd_2O_3
$Gd_2Ir_2O_7$
EuPtGe
$TmMgGaO_4$
$SrNd_2O_4$
mPDF fans
Conclusions
Table of Contents

Diffraction data for $SrNd_2O_4$ (D4c@ILL, $\lambda = 0.5$ Å)

Magnetic scattering (including diffuse) in Nd_2SrO_4 (T_N = 2.3 K)

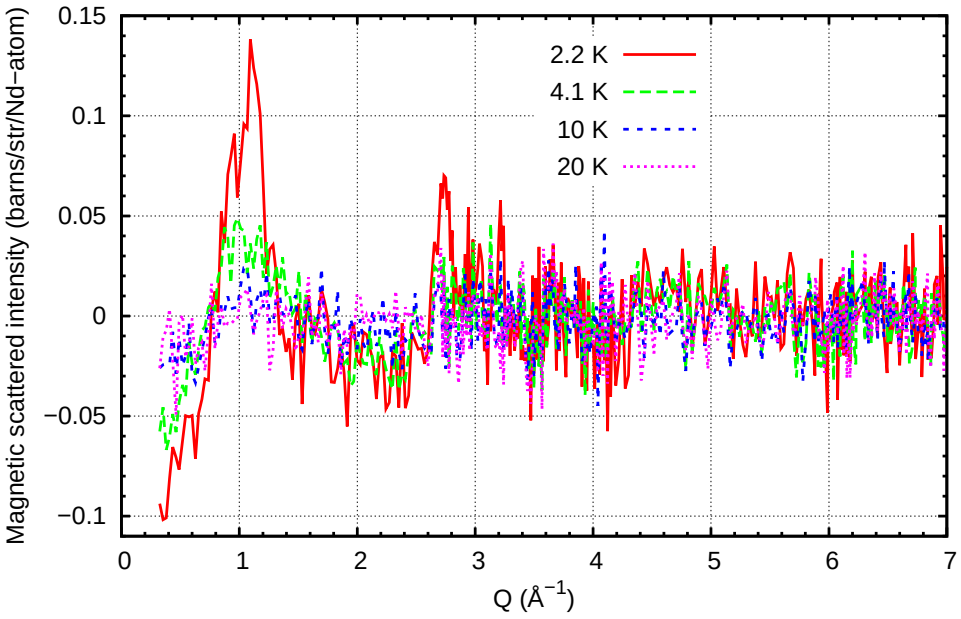

After subtraction of a 50 K "paramagnetic baseline", representing the *Q*-dependent magnetic self-scattering, and normalization via vanadium to an absolute diffraction intensity scale as $d\sigma/d\Omega$. The data are quite noisy due to the relatively small magnetic moment of Nd^{3+}.

mPDF(r) derived analytically and from RMC fits

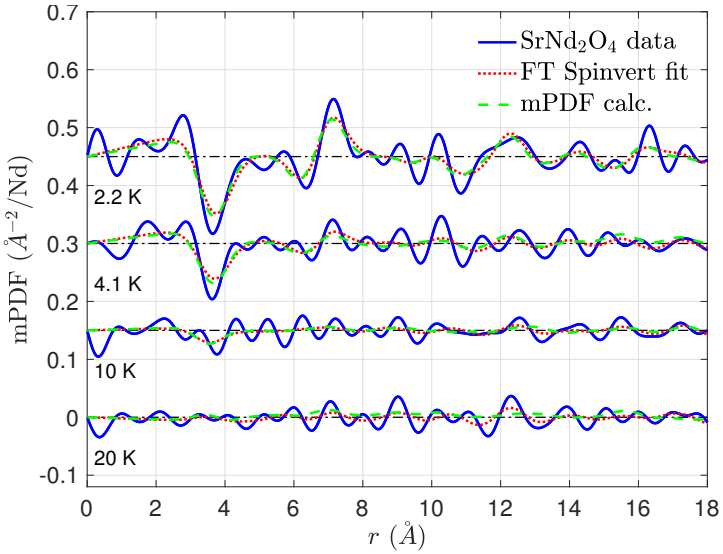

The analytical calculations of the mPDF(r) agree well with the FT of the Spinvert fits, and serve to “clean up” the effects of low counting statistics in the D4c Q-space data. The weak positive low-r slope along with the strong negative $\sim$ 3.6 Å peak confirms NN transverse AF-correlations along the 1D chains, leading to a positive NNN peak at $\sim$ 7.2 Å. The negative peak at $r \sim$ 6.2 Å indicates antiferro NNN-correlations within a hexagon (*i.e.* between the more correlated-moment Nd sites).

$SrNd_2O_4$ diffraction data (D4c@0.5Å, D20@1.3Å)

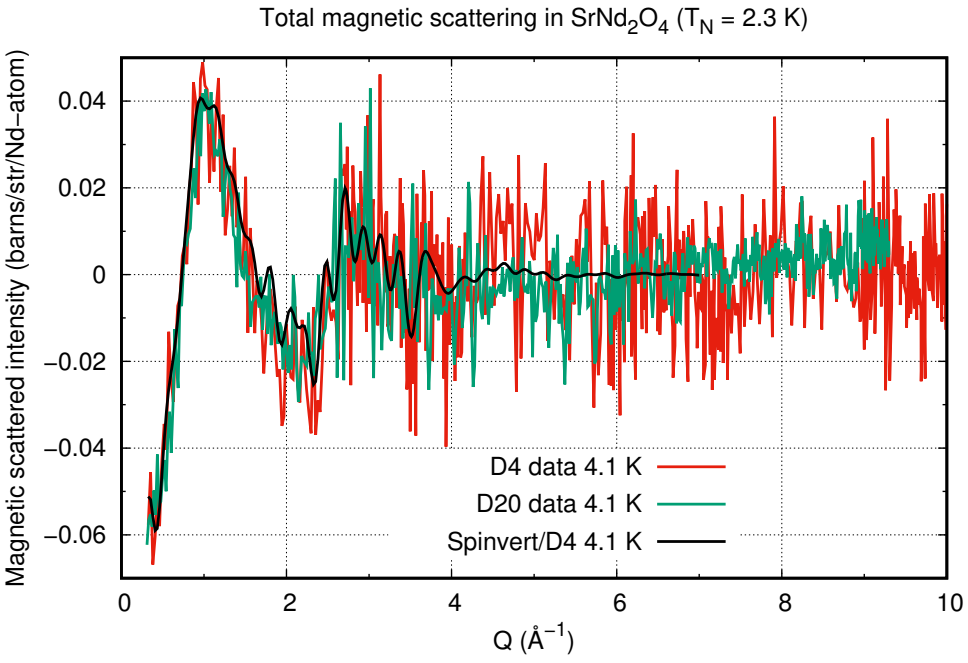

After subtraction of a 50 K “paramagnetic baseline” and equivalent normalization to an absolute intensity scale. The data from the D20 diffractometer clearly have better counting statistics, but are more sensitive to nuclear Bragg peak shifts upon temperature subtraction.

$SrNd_2O_4$ diffraction data (D4c@0.5Å, D20@1.3Å)

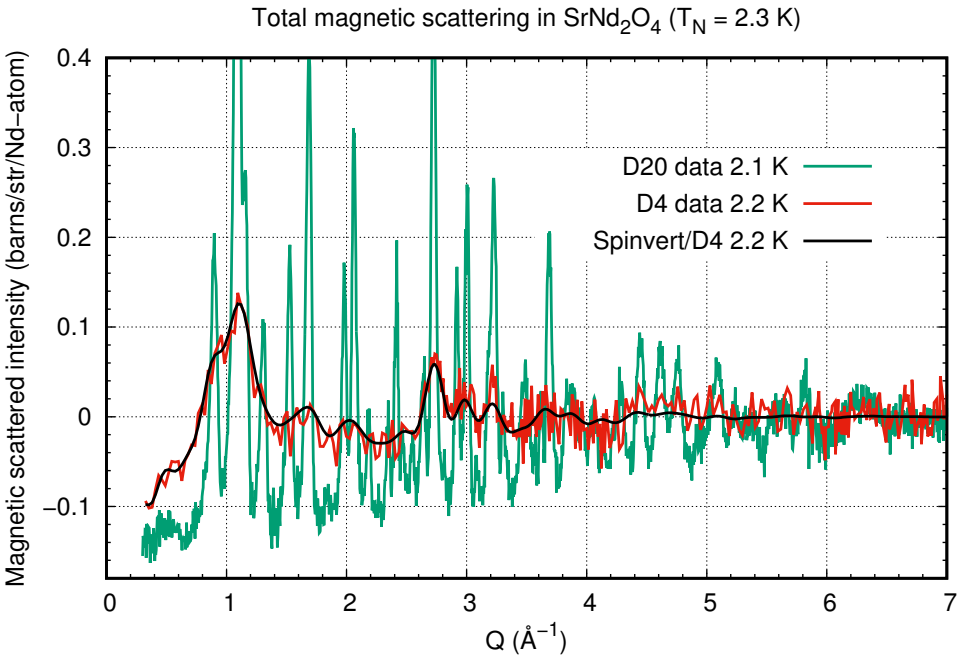

After subtraction of a 50 K "paramagnetic baseline", representing the Q-dependent magnetic self-scattering, and equivalent normalization to a vanadium standard. The data from the D20 diffractometer also have considerably (factor of 4-ish) better Q-space resolution ΔQ.

mPDF(r) data for $SrNd_2O_4$ (D4c@0.5Å, D20@1.3Å)

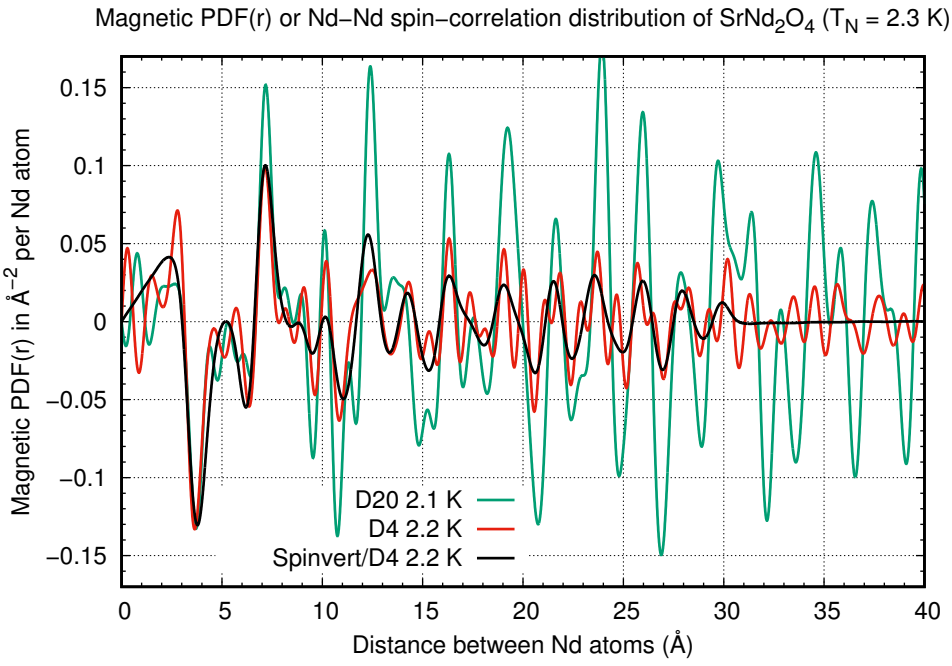

Fourier transform for $Q_{\max} = 7$ Å^{-1} after dividing by the magnetic self-scattering $\frac{2}{3}p^2\mu^2$ (*i.e.* sans form factor squared $f^2(Q)$). For this experiment, the D20 results clearly have an improved signal/noise and also a greater $R_{\max} = (5.55/2)/\Delta Q$ as compared to the D4 results.

Collaborators in developing magnetic PDF-analysis

mPDF-analysis
Henry E. Fischer
Diffraction basics
PDF-analysis
PDF examples
UO_2
carbon
mPDF-analysis
mPDF examples
$SrGd_2O_4$
Gd_2O_3
$Gd_2Ir_2O_7$
EuPtGe
$TmMgGaO_4$
$SrNd_2O_4$
mPDF fans
Conclusions
Table of Contents

Acknowledgements to (among others):

France
Navid Qureshi (ILL)
Thomas Hansen (ILL)
Andrew Wildes (ILL)
Lucile Mangin-Thro (ILL)
Gabriel Cuello (ILL)
Lionel Desgranges (Cadarache)
Virginie Simonet (CNRS Grenoble)
Elsa Lhotel (CNRS Grenoble)
Emily Lefrançois (ESRF)
Claire Colin (CNRS Grenoble)
Pierre Bordet (CNRS Grenoble)

Germany
Gerry Lander (JRC, Karlsruhe)
Roberto Caciuffo (JRC, Karlsruhe)
Silvia Seiro (IFW-Dresden)

USA
Ben Frandsen (Brigham Young U.)
Simon Billinge (Columbia U.)
Joe Paddison (ORNL, Oak Ridge)
Simon Riberolles (Iowa State U.)

UK
Oleg Petrenko (Warwick U.)
Laurent Chapon (Diamond)
Maria Diaz-Lopez (Diamond)
Ross Stewart (ISIS)

Argentina
Diego Franco (Bariloche)

Russia
Andrei Gubkin (Ekaterinburg)

Conclusions

mPDF-analysis
Henry E. Fischer
Diffraction basics
PDF-analysis
PDF examples
UO_2
carbon
mPDF-analysis
mPDF examples
$SrGd_2O_4$
Gd_2O_3
$Gd_2Ir_2O_7$
EuPtGe
$TmMgGaO_4$
$SrNd_2O_4$
mPDF fans
Conclusions
Table of Contents

Suggested new keyword for mPDF-analysis:

For the past couple years, about 2 or 3 ILL beamtime proposals have been submitted, per proposal round, that make use of magnetic PDF-analysis. Given the likely growth of this area in the near future, a new keyword in College 6 would seem warranted:

College 6 : Structure and Dynamics of Disordered Systems
$\Rightarrow$ **6-08** : magnetic PDF-analysis, static or dynamic **short**-range spin-spin correlations from magnetic diffuse scattering

And to make clear the distinction with an existing keyword of College 5B, one could modify it as:

College 5B : Magnetic structures
$\Rightarrow$ **5-32** : magnetic defects, **medium**-range order or correlations

so that 5-32 would focus more on the SANS aspects, involving longer length scales than that probed by PDF-analysis. Amorphous magnets could then be moved from 5-32 into 6-08 since the short correlation lengths are amenable to PDF-analysis.

Overall Summary and Conclusions

Magnetic diffuse total-scattering as measured by neutron diffraction provides quantitative information on short-ranged spin-spin correlations that can be either static (below T_N) or dynamic (above T_N). In contrast, Rietveld refinement provides structural information only as averaged over time and space, very useful for crystallography.

By imposing a physical 3D model of the magnetic system, RMC simulations of magnetic diffuse scattering data allow to derive in a robust way the real-space spin-spin correlation function $\langle \mathbf{S}(0) \cdot \mathbf{S}(r) \rangle$ as a function of interspin distance and temperature, even when the diffraction data are beset by significant statistical noise.

Magnetic PDF-analysis provides a *model-independent* real-space function mPDF(r), obtained directly from the diffraction data, that permits to distinguish longitudinal vs transverse spin-spin correlations, albeit with limited R-space resolution due to the magnetic form factor.

The complementary use of RMC simulations with mPDF-analysis of magnetic diffuse scattering data offers a powerful tool for investigating both static and dynamic spin-spin correlations in disordered magnetic systems, such as those subject to geometrical frustration.

Table of Contents